A Translational Polarization Rotator

David T. Chuss,[1,*] Edward J. Wollack,[1] Giampaolo Pisano,[2], Sheridan Ackiss,[3]
Kongpop U-Yen,[1] Ming wah Ng[2]

[1] *Observational Cosmology Laboratory, Code 665, NASA Goddard Space Flight Center,
Greenbelt, MD 20771, USA*

[2] *University of Manchester, Manchester, UK*

[3] *Georgia Tech, Atlanta, GA, USA*

Corresponding author: David.T.Chuss@nasa.gov

We explore a free-space polarization modulator in which a variable phase
introduction between right- and left-handed circular polarization components
is used to rotate the linear polarization of the outgoing beam relative to that
of the incoming beam. In this device, the polarization states are separated
by a circular polarizer that consists of a quarter-wave plate in combination
with a wire grid. A movable mirror is positioned behind and parallel to the
circular polarizer. As the polarizer-mirror distance is separated, an incident
linear polarization will be rotated through an angle that is proportional to the
introduced phase delay. We demonstrate a prototype device that modulates
Stokes Q and U over a 20% bandwidth.

OCIS codes: 350.1270, 120.5410, 230.4110, 240.5440, 050.6624.

1. Introduction

Polarization modulation is the systematic mapping of an incident polarization state into a
new polarization state for subsequent demodulation and detection. This technique is useful
for polarimetric applications in which the polarization signal is significantly smaller than the
unpolarized background signal. Relevant applications include polarization contrast imaging
and astronomical polarimetry [1].

It is desirable for the polarization modulator to vary the polarization state but not the
total amount of polarization. That is, in terms of Stokes parameters, an ideal modulator is
subject to the condition

$$Q^2 + U^2 + V^2 = \text{constant}. \tag{1}$$

This condition corresponds to a modulator that does not change the total coherence of the signal and makes the problem of measuring the polarization experimentally cleaner. Modulators that satisfy this condition are represented by unitary Jones matrices. In the homomorphically-equivalent Mueller formalism, the matrix representations of such modulators are orthogonal. This restriction limits the non-trivial operations to either a physical rotation or an introduction of a phase delay between orthogonal polarization components. Such operations are represented by rotations on the Poincaré Sphere [2] in which the basis and magnitude of the phase delay determine the axis and magnitude of the rotation, respectively.

Apart from the trivial example of instrument rotation, modulators typically vary either the basis of the system or the phase between two orthogonal polarizations. Figure 1 shows modulation topologies for a selection of unitary modulators and their representations on the Poincaré Sphere. Corresponding Mueller matrices are also shown. Figure 1A shows a modulation scheme in which a constant phase delay of π is introduced between two linear orthogonal polarizations. Modulation is accomplished by systematically changing the basis of phase separation in the $Q - U$ plane. A quasioptical realization of this topology is the rotating half-wave plate [3–5]. Topologically equivalent waveguide implementations are also possible [6]. For ideal devices, it is possible to completely modulate linear polarization for a detector that is sensitive to linear polarization.

Similarly, for measurement of circular polarization using a detector sensitive to linear polarization, it is possible to introduce a constant phase delay of $\pi/2$ between linear orthogonal polarizations and changing the basis of separation as shown in Figure 1B. Rotating quarter-wave plates and birefringent waveguides are examples of this architecture [7].

Alternatively, as shown in Figure 1C, it is possible to hold the polarization basis constant while introducing a variable phase delay between two orthogonal linear polarizations. A quasioptical example of this is the variable-delay polarization modulator (VPM). VPMs have been utilized to modulate polarization [8–10] and have the potential to produce low and controllable systematic errors [11] using small translational motions. This is a potential advantage for space flight applications as this concept can be realized with high reliability flexures that eliminate the need for rotational bearings. VPMs can only modulate a single linear Stokes parameter and therefore must rely on other degrees of freedom such as instrument rotation or separate optical paths in order to fully modulate both Q and U. For large telescopes, instrument rotation may lead to undesirable observational constraints, modulated instrumental polarization, or incomplete polarization coverage in the final data products. Thus it is desirable to seek a solution that fully modulates linear polarization in a single element.

Introduction of a variable phase (Fig. 1D) between the two *circular* polarization states

2

A

Topology: π phase delay between linear states; basis of phase separation is rotated
Free-space Example: Rotating Half-wave plate
Waveguide Example: Rotating Waveguide & π differential phase shifter

$$\begin{bmatrix} 1 & 0 & 0 & 0 \\ 0 & \cos 4\theta & -\sin 4\theta & 0 \\ 0 & \sin 4\theta & \cos 4\theta & 0 \\ 0 & 0 & 0 & 1 \end{bmatrix}$$

B

Topology: $\pi/2$ phase delay between linear states; basis of phase separation is rotated
Free-space Example: Rotating Quarter-wave plate
Waveguide Example: Rotating Waveguide & $\pi/2$ differential phase shifter

$$\begin{bmatrix} 1 & 0 & 0 & 0 \\ 0 & \cos^2 2\theta & -\tfrac{1}{2}\sin 4\theta & -\sin 2\theta \\ 0 & \tfrac{1}{2}\sin 4\theta & -\sin^2 2\theta & \cos 2\theta \\ 0 & \sin 2\theta & -\cos 2\theta & 0 \end{bmatrix}$$

C

Topology: variable phase delay (δ) between linear states; basis of phase separation is fixed.
Free-space Example: Variable-delay Polarization Modulator
Waveguide Example: $\pi/2$ differential phase shifter & Faraday Rotator with delay δ.

$$\begin{bmatrix} 1 & 0 & 0 & 0 \\ 0 & \cos \delta & 0 & -\sin \delta \\ 0 & 0 & 1 & 0 \\ 0 & \sin \delta & 0 & \cos \delta \end{bmatrix}$$

D

Topology: variable phase delay (δ) between circular states; basis of phase separation is fixed.
Free-space Example: Translational Polarization Rotator (TPR)
Waveguide Example: Faraday Rotator with delay δ.

$$\begin{bmatrix} 1 & 0 & 0 & 0 \\ 0 & \cos \delta & -\sin \delta & 0 \\ 0 & \sin \delta & \cos \delta & 0 \\ 0 & 0 & 0 & 1 \end{bmatrix}$$
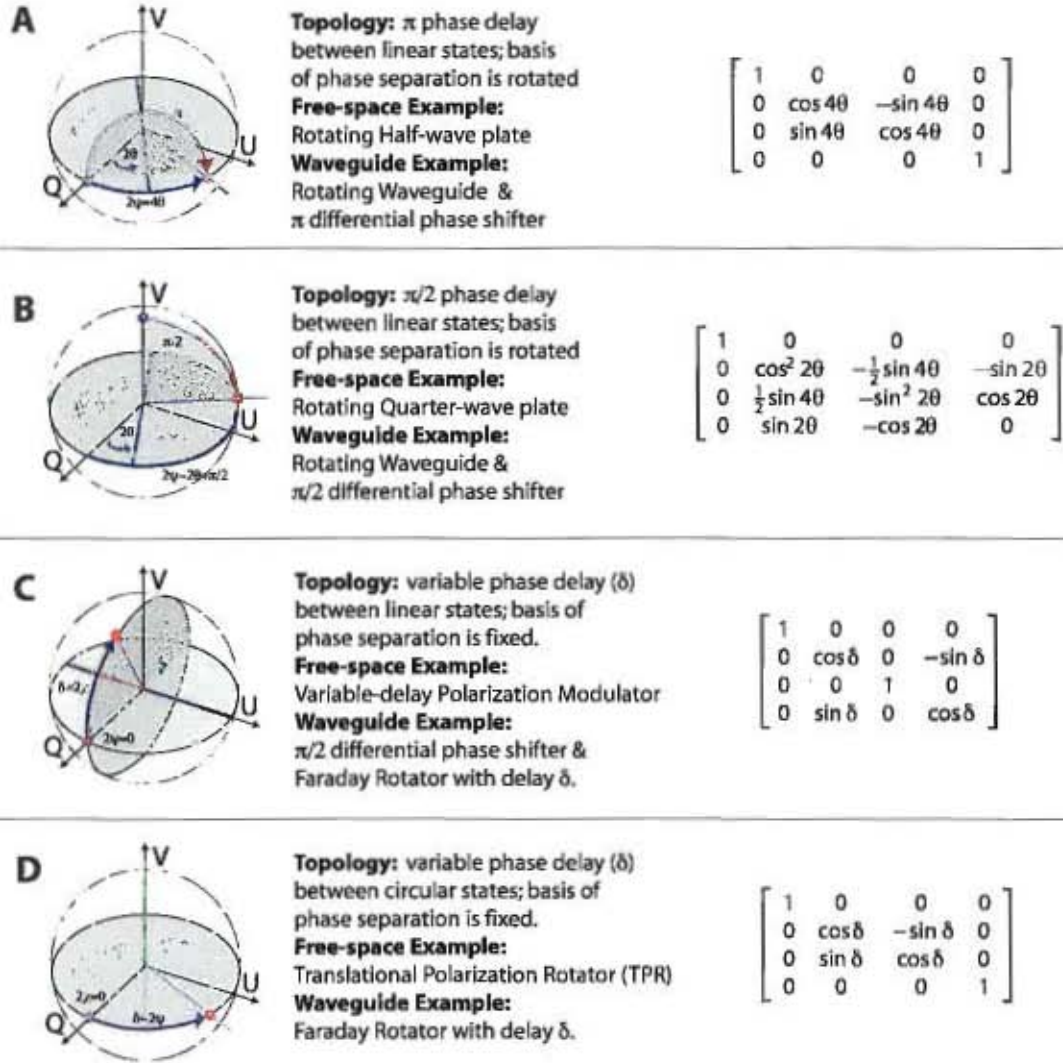
Fig. 1. Selected matrix elements for several ideal polarization modulators on the Poincaré Sphere are shown. The green line shows the axis connecting the two polarization states between which a phase delay, δ, is introduced. Violet and dots indicate the initial and final polarization states, respectively. Blue arrows indicate the modulation path on the sphere. Red arrows indicate static phase delays. Deviations from ideal behavior are generally caused by finite bandwidth, biattenuance, differential reflection, etc. The orthogonal Mueller matrix for each architecture is shown on the right.

3

provides a means to fully modulate linear polarization. An example of this is implemented in a waveguide is a Faraday Rotator [12–14] having a variable phase delay. In this case, the circular birefringence of ferrite material is altered as a function of applied magnetic field.

In this paper, we present a concept for achieving a non-magnetic free-space modulator using topology 'D'. We accomplish this by separating the two circular polarization states and introducing a variable and differential phase delay. We refer to this device as a Translational Polarization Rotator or TPR. Our implementation is related to the VPM architecture. In Section 2 we describe an implementation of a TPR. In Section 3 we report testing of a prototype TPR. We summarize in Section 4.

2. The TPR
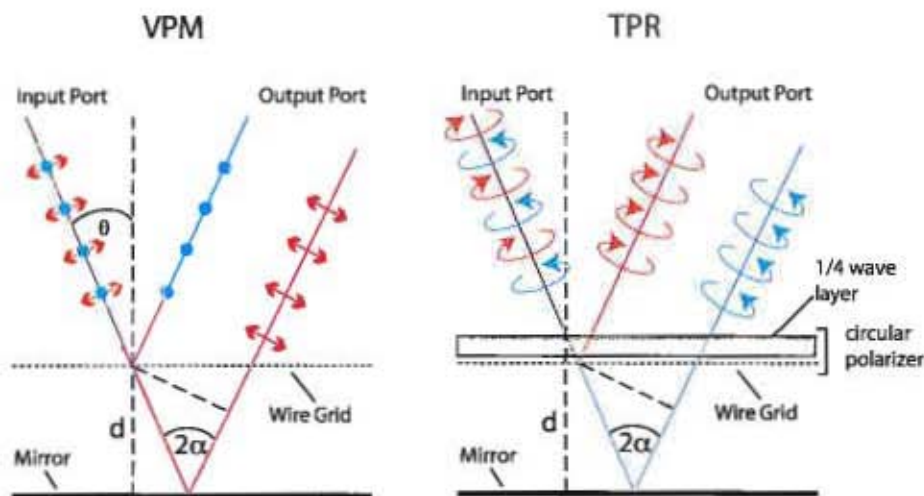
Fig. 2. The topology for the TPR compared with the VPM is shown. The TPR consists of a circular polarizer placed in front of and parallel to a movable mirror and introduces a variable phase delay between the orthogonal circular polarization states.

To realize a variable phase delay between right- and left-handed circular polarization components in a beam of radiation, we employ the architecture illustrated on the right side of Figure 2. This device consists of a quarter-wave plate placed in front of a VPM with its fast (or slow) axis oriented at a 45° angle with respect to the VPM polarizer direction. The quarter wave plate converts incoming circular polarization states to orthogonal linear polarizations. The VPM then introduces a variable phase delay between the linear polarizations. As the beam exits the device, another pass through the quarter wave plate converts the linear polarizations back to right- and left- circular.

4

For purposes of explanation, the TPR system can be analyzed using Jones matrice [15]. This simple analysis that follows is an ideal approach that is intended to illustrate the basic functionality of the TPR. The appropriateness of this basic approach relies on the absence of multiple coherent reflections or standing waves between the constituent elements of the TPR. Use of transfer matrices enables a more general treatment without this limitation [10].

We present the analysis of a VPM oriented at an arbitrary angle with respect to a general wave plate. At the end, we can set the wave plate's phase delay and the angle between the wave plate and VPM appropriately to realize the desired modulation.

The Jones matrix for the TPR can be written as

$$\overline{J}_{TPR} = \overline{J}_{WP}(0,\beta)\overline{J}_{VPM}(\theta,\delta)\overline{J}_{WP}(0,\beta). \tag{2}$$

Here, $\overline{J}_{WP}(0,\beta) = \overline{\Delta}(\beta)$ represents the effect on the incoming radiation when passing through the wave plate on the input side of the device. The angular coordinate system is chosen such that the wave plate's fast axis is aligned with the zero angle. θ is the angle of the VPM wires with respect to the fast axis of the wave plate, and β is the phase delay between two orthogonal linear polarizations introduced by the wave plate. The phase delay introduced by the VPM is δ. The Jones matrix for the VPM is then $\overline{J}_{VPM}(\theta,\delta) = \overline{R}(\theta)\overline{\Delta}(\delta)\overline{R}(\theta)$.

The wave plate and VPM can be approximated by simple expressions and thus,

$$\overline{J}_{TPR} = \overline{\Delta}(\beta)\left[\overline{R}(\theta)\overline{\Delta}(\delta)\overline{R}(\theta)\right]\overline{\Delta}(\beta) \tag{3}$$

where

$$\overline{R}(\theta) = \begin{pmatrix} \cos\theta & \sin\theta \\ -\sin\theta & \cos\theta \end{pmatrix}, \overline{\Delta}(\delta) = \begin{pmatrix} e^{i\delta/2} & 0 \\ 0 & e^{-i\delta/2} \end{pmatrix} \tag{4}$$

are the Jones representations of a rotation by an angle θ and an introduction of phase δ between two orthogonal linear polarizations, respectively. Note that because the VPM operates in reflection, there is a mapping between $\theta \to -\theta$ between the input and output direction, resulting in the proper transformation being $\overline{R}(\theta)\overline{\Delta}(\delta)\overline{R}(\theta)$ rather than $\overline{R}(-\theta)\overline{\Delta}(\delta)\overline{R}(\theta)$.

Substituting appropriately, one finds,

$$\overline{J}_{TPR} = \begin{pmatrix} e^{i\beta}(e^{i\delta/2}\cos^2\theta - e^{-i\delta/2}\sin^2\theta) & \sin 2\theta\cos\delta/2 \\ -\sin 2\theta\cos\delta/2 & e^{-i\beta}(-e^{i\delta/2}\sin^2\theta + e^{-i\delta/2}\cos^2\theta) \end{pmatrix}. \tag{5}$$

We next calculate the polarization transfer function for Stokes U polarization state using the density matrix

$$\overline{J}_{TPR}^\dagger \overline{\sigma}_2 \overline{J}_{TPR}. \tag{6}$$

This result can be decomposed in the Pauli basis [1]:

$$D = I\overline{\sigma_0} + Q\overline{\sigma_1} + U\overline{\sigma_2} + V\overline{\sigma_3} = I\begin{pmatrix} 1 & 0 \\ 0 & 1 \end{pmatrix} + Q\begin{pmatrix} 1 & 0 \\ 0 & -1 \end{pmatrix} + U\begin{pmatrix} 0 & 1 \\ 1 & 0 \end{pmatrix} + V\begin{pmatrix} 0 & -i \\ i & 0 \end{pmatrix}. \tag{7}$$

5

The result of these manipulations is the following transformation.

$$
\begin{aligned}
U \rightarrow & 2\sin 2\theta \cos \delta/2 \left[\cos^2 \theta \cos\left(\beta + \delta/2\right) - \sin^2 \theta \cos\left(\beta - \delta/2\right)\right] Q \\
& + \left[-\sin^2 2\theta \cos^2 \delta/2 - 2\cos^2 \theta \sin^2 \theta \cos 2\beta - \cos 2\theta \sin \delta \sin 2\beta + \cos 2\beta \cos \delta(\sin^4 \theta + \cos^4 \theta)\right] U \\
& + \left[\sin 2\beta \left\{2\cos^2 \theta \sin^2 \theta - \cos \delta(\sin^4 \theta + \cos^4 \theta)\right\} - \cos 2\beta \sin \delta \cos 2\theta\right] V. \qquad (8)
\end{aligned}
$$

The coefficients of the Stokes Parameters are the elements of the third column of the Mueller matrix (or the third row of the inverse Mueller matrix). Substituting $\theta = \pi/4$ and $\beta = \pi/2$, one obtains

$$
U \rightarrow Q' \sin \delta - U' \cos \delta. \qquad (9)
$$

This is the desired transformation and demonstrates that the architecture described for the TPR does indeed inject a variable phase delay between left- and right- circular polarization. It is convenient to think in terms of Equation 9 as representing a polarimeter in transmission with the polarized detectors oriented at 45° with respect to the optical axis of the quarter-wave plate. The effect of the modulator is to vary the polarization sensitivity of the detector system as a function of the gird-mirror delay, δ.

3. Measurement

A prototype TPR has been constructed using a dielectrically-embedded metal mesh quarter wave plate of the type presented in [16,17]. This was mounted to the front of a VPM nearly identical to the Hertz prototype [9, 10] (see Fig. 3), and the grid-mirror separation was controlled using a manual linear micrometer stage. The metal mesh quarter wave plate is based on photolithographic techniques used in the past to realize half-wave plates [18]. This device provides a phase shift between orthogonal linear polarizations of 89.2° ± 1.5° over a 40% bandwidth (75-110 GHz). The transmittance for the two polarizations is matched to 2% from 77-94 GHz where we experimentally concentrate our efforts. The biattenuance of the wave plate in this configuration leads to modulated instrumental polarization, and so the bandwidth has been limited to control this effect.

To test the operation of the TPR, the prototype was included in the test setup shown in Figure 4. This largely follows the experimental approach utilized in [10]. The test setup used a pair of feed horns to couple the quasioptical testbed to an Agilent PNA-X vector network analyzer. Microwaves polarized in the vertical ($-U$) direction are transmitted from Port 1 (designated the "Source"). A polarizing wire grid was used to further define the polarization state and served to redirect the radiation to an ellipsoidal mirror that maps the feed's beam waist onto the TPR. A second, identical ellipsoidal mirror re-mapped the beam waist into a second feed horn (the "Detector") attached to Port 2 of the PNA-X. Orthomode Transducers (OMT) were used to terminate the unused polarization in each feed horn. The quarter-wave
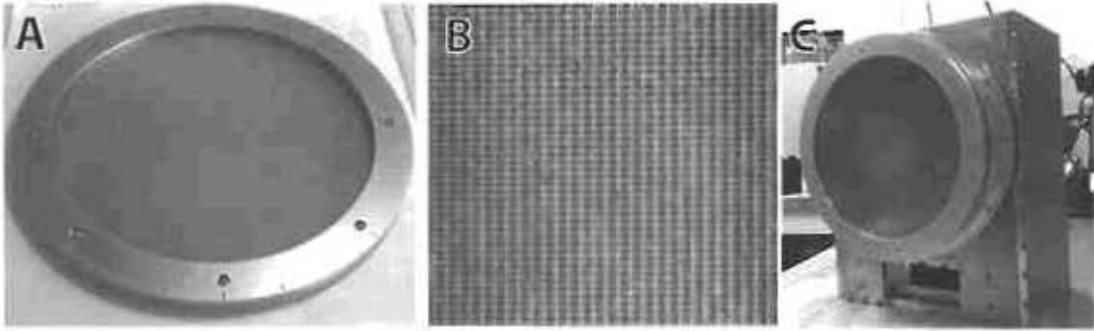
6

Fig. 3. The metal-mesh wave plate is shown (A) along with a close-up view of its surface (B). The prototype TPR is shown in (C).

plate was tilted at an angle $> 5°$ with respect to the VPM wire grid, to avoid trapped modes inside of the TPR.

A second linear micrometer stage was inserted between the TPR and the test setup. This linear stage was used to vary the position of the TPR ("B" in Figure 4) relative to the rest of the optics. By taking measurements of the response at different positions of the TPR, it was possible to use the varied phase to separate the TPR response from that of the rest of the optics using a procedure similar to that outlined by Eimer et al. [19]. Thus each S_{21} scattering parameter measurement described below is a composite of four measurements taken at 400 μm intervals for the TPR position.

We characterized the polarization transfer function of the TPR by measuring the normalized linear Stokes parameters, $q \equiv Q/I$ and $u \equiv U/I$, at Port 2. This was done by measuring the complex S_{21} scattering parameter as a function of grid-mirror separation at four rotations of the horn attached to Port 2: $0°$ (V), $90°$ (H), $45°$ (D_-), and $-45°$ (D_+). These angles were measured at the feed horn flange and their relative error is roughly $\pm 1°$. To mechanically facilitate coupling to the millimeter-wave receiver module, a short (1.5-inch) section of appropriate waveguide twist between was used between Port 2 and the OMT for measurements of H, D_-, and D_+. The Stokes parameters can be extracted from these measurements.

$$u(d) = \frac{H(d) - f_u V(d)}{H(d) + f_u V(d)} \tag{10}$$

$$q(d) = \frac{D_+(d) - f_q D_-(d)}{D_+(d) - f_q D_-(d)}. \tag{11}$$

The values f_q and f_u are the relative gain of the system between the different rotations. The gain upon rotation due to changes in the feed illumination or waveguide twist ohmic loss. The D_+ and D_- measurements each employ 1.5 inch twists, so we set $f_q = 1$. The measurements
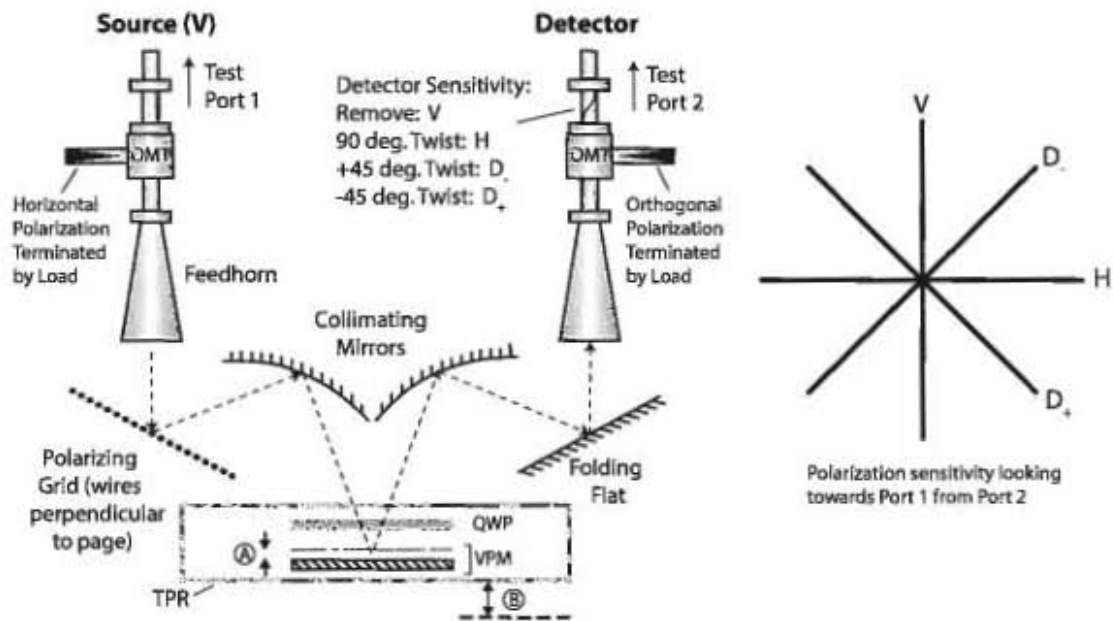
Source (V)

Test Port 1

OMT

Horizontal Polarization Terminated by Load

Feedhorn

Detector

Detector Sensitivity:
Remove: V
90 deg. Twist: H
+45 deg. Twist: D.
-45 deg. Twist: D.

Test Port 2

OMT

Orthogonal Polarization Terminated by Load

Collimating Mirrors

Polarizing Grid (wires perpendicular to page)

Folding Flat

QWP

VPM

TPR

Ⓐ

Ⓑ

V

D.

H

D.

Polarization sensitivity looking towards Port 1 from Port 2

Fig. 4. The test setup used to validate the VPM is shown (left). The grid–mirror separation is given by A, and the overall displacement of the TPR is given by B. The rotational coordinate system used for the polarization measurements is shown on the right.

8

of V do not include a twist section, while those for H do. Therefore, to account for the loss imbalance in the measurement of V relative to that of H, $f_u = 0.99$.

The calibrated measurements have been integrated over the 77-94 GHz band and are shown in Figure 5. The model responses for q and u are the terms in equation 9 integrated over the bandwidth. Because the wavelength is much greater the diameter of the wire of the polarizing grid, the phase can be approximated by $4\pi d \cos \alpha / \lambda$ where d is the grid-mirror separation, $\alpha = 20°$ is the incidence angle of the radiation on the modulator, and λ is the wavelength [10].
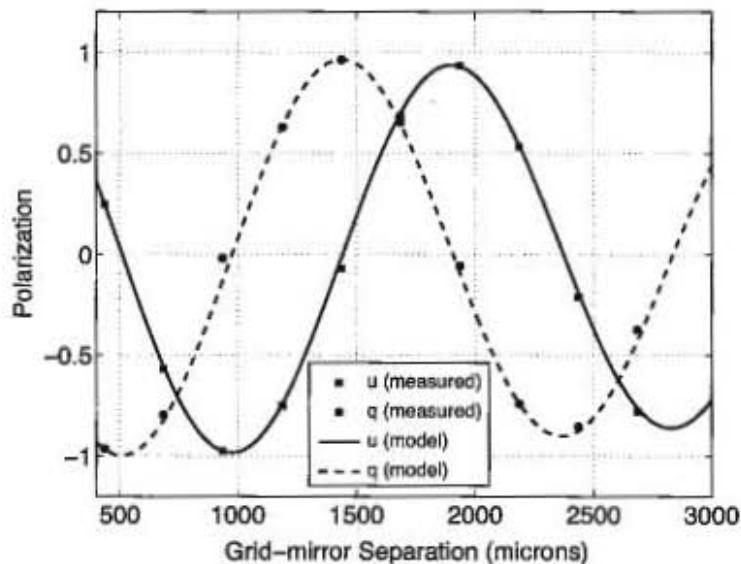

Fig. 5. The response of the TPR to an incident $-u$ (vertically-polarized) signal is shown. The measured q and u response for the integrated 77-94 GHz response is superposed on the integrated response expected from theory.

4. Discussion

A prototype TPR has been constructed and validated using a vector network analyzer. Residual deviations from the expected behavior are likely due to either gain uncertainty, biattenuance in the quarter-wave plate, an insufficiently accurate model for the polarizing grid, and/or residual trapped modes between the quarter-wave plate and the VPM. The characteristics of the circular polarizer will ultimately determine the TPR's performance as a polarization modulator. The demonstrated approach is potentially useful for astronomical polarimetry in the millimeter through far-infrared in that it enables full linear polarization modulation with a single reflective element that utilizes small linear motions.

References

1. C. Brosseau, *Fundamentals of Polarized Light* (John Wiley & Sons, 1998).

2. J. Tinbergen, *Astronomical Polarimetry* (Cambridge University Press, 1996).

3. R.H. Hildebrand, J.A. Hildebrand, J.L. Dotson, C.D. Dowell, G. Novak, & J.E. Vaillancourt, "A Primer on Far-Infrared Polarimetry" Publications of the Astronomical Society of the Pacific **112**, 1215–1235 (2000).

4. G. Savini, G. Pisano, & P. A. R. Ade, "Achromatic half-wave plate for submillimeter instruments in cosmic microwave background astronomy: modeling and simulation" Appl. Opt. **45**, 8907–8915 (2006).

5. S.A. Bryan, T.E. Montroy, & J.E. Ruhl, "Modeling dielectric half-wave plates for cosmic microwave background polarimetry using a Mueller matrix formalism", Applied Optics **49**, 6313–6323 (2010).

6. G. Pisano, S. Melhuish, G. Savini, L. Piccirillo, & B. Maffei, *A Broadband W-Band Polarization Rotator With Very Low Cross Polarization*, IEEE Microwave and Wireless Components Letters **21**, 127–129 (2011).

7. S. Pancharatnam, "Achromatic combinations of birefringent platesPart II. An achromatic quarter wave plate", Proc. Indian Acad. Sci., Sect. A **42**, 24–31 (1955).

8. D. T. Chuss, E. J. Wollack, S. H. Moseley, & G. Novak, "Interferometric polarization control," Applied Optics **45**, 5107–5117 (2006).

9. M. Krejny, D. Chuss, C. Drouet d'Aubigny, D. Golish, M. Houde, H. Hui, C. Kulesa, R. F. Loewenstein, S. H. Moseley, G. Novak, G. Voellmer, C. Walker, & E. Wollack, "The Hertz/VPM polarimeter: Design and first light observations," Applied Optics **47** 4429–4440 (2008).

10. D. T. Chuss, E. J. Wollack, R. Henry, H. Hui, A. J. Juarez, M. Krejny, S. H. Moseley, & G. Novak, "Properties of a Variable-delay Polarization Modulator," Applied Optics **51**, 197–208 (2012).

11. D. T. Chuss et al., "The Primordial Inflation Polarization Explorer (PIPER)", Proc. SPIE **7741**, 77411P-1 (2010).

12. G. P. Nanos, "Polarization of the blackbody radiation at 3.2 centimeters", The Astrophysical Journal **232**, 341–347 (1979).

13. P.A.R. Ade, D.T. Chuss, S. Hanany, V. Haynes, B.G. Keating, A. Kogut, J.E. Ruhl, G. Pisano, G. Savini, & E.J. Wollack, "Polarization Modulators for CMBPol", Journal of Physics: Conference Series **155**, 012006 (2009).

14. A.C. Gault, E.M. Bierman, P.O. Hyland, B.G. Keating, S.S. Malu, & P.T. Timbie, "Measurements of a Cryogenic Linear Polarization Modulator for mm-Wavelengths", IEEE Microwave and Wireless Components Letters **99**, 1 (2012).

15. R. Jones, "New calculus for the treatment of optical systems," J. Opt. Soc. Am. **31**, 488–493 (1941).

16. G. Pisano, M. W. Ng, V. Haynes, & B. Maffei, "A Broadband Photolithographic Polariser for Millimetre Wave Applications", PIERS Proceedings, Kuala Lumpur, Malaysia, 1748–1751 (2012).

17. B. Maffei, G. Pisano, Ming Wah Ng & Vic Haynes, "Millimetre Wave Photolithographic Polariser Beam Impact", PIERS Proceedings, Kuala Lumpur, Malaysia, 1761–7165 (2012).

18. G. Pisano, G. Savini, P. Ade, & V. Haynes, "A Metal-mesh Achromatic Half-Wave Plate for use at Submillimetre Wavelengths", Applied Optics, **47**, 6251-6256 (2008).

19. J.R. Eimer, C.L. Bennett, D.T. Chuss, and E.J. Wollack, "Vector Reflectometry in a Beam Waveguide", Review of Scientific Instruments **82**, 086101 (2011).